

Article

Ground-Based Measurements of Cloud Properties at the Bucharest–Măgurele Cloudnet Station: First Results

Răzvan Pîrloagă^{1,2}, Dragoș Ene^{1,†}, Mihai Boldeanu^{1,‡}, Bogdan Antonescu^{1,*}, Ewan J. O'Connor³ and Sabina Ștefan²

¹ Remote Sensing Department, National Institute of Research and Development for Optoelectronics INOE 2000, Str. Atomîștilor 409, RO077125 Măgurele, Romania

² Faculty of Physics, University of Bucharest, Str. Atomîștilor 405, RO077125 Măgurele, Romania

³ Finnish Meteorological Institute, 00560 Helsinki, Finland

* Correspondence: bogdan.antonescu@inoe.ro

† Currently at: ERATOSTHENES Centre of Excellence, Saripolou 2-6, 3036 Limassol, Cyprus.

‡ Currently at: Speech and Dialogue Research Laboratory, Faculty of Electronics, Telecommunications and Information Technology, University Politehnica of Bucharest, 060042 Bucharest, Romania.

Abstract: Data collected over a period of 18 months (December 2019–May 2021) at the Bucharest–Măgurele Cloudnet station were analysed for the first time to determine the macrophysical and microphysical cloud properties over this site. A total number of 1,327,680 vertical profiles containing the target classification based on the Cloudnet algorithm were analysed, of which 1,077,858 profiles contained hydrometeors. The highest number of profiles with hydrometeors (>60%) was recorded in December 2020, with hydrometeors being observed mainly below 5 km. Above 5 km, the frequency of occurrence of hydrometeors was less than <20%. Based on the initial Cloudnet target classification, a cloud classification scheme was implemented. Clouds were more frequently observed during winter compared with other seasons (45% of all profiles). Ice clouds were the most frequent type of cloud (468,463 profiles) during the study period, followed by mixed phases (220,280 profiles) and mixed phased precipitable clouds (164,868 profiles). The geometrical thickness varied from a median value of 244 m for liquid clouds during summer to 3362 m for mix phased precipitable clouds during spring.

Keywords: cloud; radar; climatology



Citation: Pîrloagă, R.; Ene, D.; Boldeanu, M.; Antonescu, B.; O'Connor, E.J.; Ștefan, S. Ground-Based Measurements of Cloud Properties at the Bucharest–Măgurele Cloudnet Station: First Results. *Atmosphere* **2022**, *13*, 1445. <https://doi.org/10.3390/atmos13091445>

Academic Editor: Bryan C. Weare

Received: 5 July 2022

Accepted: 3 September 2022

Published: 6 September 2022

Publisher's Note: MDPI stays neutral with regard to jurisdictional claims in published maps and institutional affiliations.



Copyright: © 2022 by the authors. Licensee MDPI, Basel, Switzerland. This article is an open access article distributed under the terms and conditions of the Creative Commons Attribution (CC BY) license (<https://creativecommons.org/licenses/by/4.0/>).

1. Introduction

Clouds exert a significant effect on the Earth's radiation budget and thus on Earth's climate. This effect is modulated by the temporal and spatial distribution of clouds and by their macrophysical (e.g., height, thickness) and microphysical (e.g., phase, particle size distribution) properties [1,2]. To obtain a detailed understating of the macrophysical and microphysical properties of clouds, long-term high-resolution spatial and temporal observations are required. These high-resolution observations can be obtained from different satellite and ground-based instruments (e.g., cloud radars) and also by the synergistic use of multiple instruments from ground-based remote sensing stations.

Observations of cloud characteristics have been collected from around the globe during land-based, ship-borne, and airborne intense observation campaigns (e.g., [3]). Longer-term continuous characterisation of clouds have been provided by ground-based observation facilities (e.g., JOYCE–Jülich Observatory for Cloud Evolution [4], SIRTAs–Site Instrumental de Recherche par Télédétection Atmosphérique [5]), satellite missions aiming to measure clouds and aerosols (e.g., CloudSat and CALIPSO [6], CERES–Clouds and the Earth's Radiant Energy System [7]) and networks for cloud observation (ARM–Atmospheric Radiation Measurement program [8], Cloudnet [9]) implemented since the 1990s.

The Cloudnet network was developed with the main purpose of combining accurate, ground-based instrument observations from several instruments to obtain continuous records of cloud variables (e.g., ice water content, liquid water content) and their associated errors and to use these observations to evaluate and improve the quality of operational forecast models [9]. Currently, Cloudnet comprises 20 stations, of which two stations, the most eastern ones in the network, Bucharest–Măgurele and Galați stations, are located in Romania (cloudnet.fmi.fi, accessed on 16 March 2022). To obtain detailed information on the vertical profile of clouds, each Cloudnet station requires the continuous operation of a cloud radar, a microwave radiometer and a ceilometer. The measurements are then synergetically combined together with thermodynamic profiles from a numerical weather prediction model within the Cloudnet algorithm suite [10], developed and implemented within the Cloudnet project and then extended within the European Research Infrastructure for Aerosol, Clouds and Trace Gases, ACTRIS. One of the products provided by Cloudnet is the target classification, which gives information regarding the microphysical properties of clouds [11]. Additional parameters provided by the algorithm suite include drizzle and drizzle parameters below the cloud base [12], liquid water content [13], and ice cloud microphysics [14,15].

A series of recent articles have used the Cloudnet algorithm suite to study the properties of clouds observed at different locations. Bühl et al. [16] studied the ice- and liquid-water properties in mixed-phase clouds for a dataset collected at a Cloudnet station in Leipzig, Germany and processed with the Cloudnet target classification scheme. The results indicated that a detailed insight into the microphysics of mixed-phase clouds is possible with a combination of the Leipzig Aerosol and Cloud Remote Observation System (LACROS, [17]) instrumentation (PollyXT Raman/depolarisation lidar, Jenoptik ceilometer CHM15kx, MIRA-35 cloud radar, HATPRO microwave radiometer) and Cloudnet target classification. Achtert et al. [18] also used the Cloudnet target classification to investigate the properties of Arctic clouds using ship-borne observations collected over three months in the summer and autumn of 2014 during the Arctic Clouds in Summer Experiment. Their results showed that during autumn, compared to summer, mixed-phase and ice clouds are more frequently observed, and liquid clouds are less frequent at lower altitudes. Nomokonova et al. [19] further studied Arctic clouds with the first analysis of clouds over Ny Ålesund, Svalbard, using data collected by a 94 GHz cloud radar, a ceilometer and a microwave radiometer over 14 months (June 2016–July 2017). To obtain the macrophysical and microphysical properties of clouds, the Cloudnet target classification was applied. Clouds were present 82% of the time, with the highest frequency of occurrence observed in October 2016 (92%). Multi-layer clouds represented 44.8% and single-layer clouds 36%. At lower latitudes, the geometrical and microphysical properties of clouds over the Eastern Mediterranean basin were analysed with the Cloudnet target classification by Marinou et al. [20]. Observations with a PollyXT lidar, 35 GHz cloud radar, microwave radiometer and a Doppler wind lidar were performed in Finokalia, Greece, as part of the PRE-TECT experiment in April 2017. The result indicated that convective clouds were observed most frequently (58% of the cases), followed by mid-level (38%) and low-level clouds (2%).

Here, we present the properties of clouds over Bucharest–Măgurele based on the first 18 months of observations (December 2019–May 2021) at this Cloudnet station. To the authors' best knowledge, this is the first time that such a study has been performed in Romania using continuous ground-based measurements and the Cloudnet target classification. Previous cloud studies in Romania focused on the cloud cover fraction based on lidar and satellite measurements [21,22] or on the synoptic environments associated with cumulonimbus clouds based on station observation and reanalysis data [23] without providing statistical insights into the cloud microphysics. The structure of this paper is as follows. Section 2 discusses the observation dataset and the methodology (Sections 2.1–2.3) and presents the hydrometeor and cloud classification (Section 2.4). Section 3 discusses the en-

vironmental (Section 3.1), hydrometeor (Section 3.2), and cloud (Section 3.3) characteristics captured during the study period, and Section 4 concludes this article.

2. Data and Methods

This section describes the remote sensing instruments used in this study (i.e., cloud radar, microwave radiometer, and ceilometer), the datasets provided by these instruments and the methods used to analyse the datasets. All the instruments were located at the Măgurele Centre for Atmosphere and Radiation Studies (MARS), a research platform situated (44.34° N, 26.01° E, 71 m MSL) approximately 12.5 km from Bucharest, Romania (Figure 1). The Romanian plain, south of the Carpathian mountains, in which MARS is situated, is characterised by hot summers and a humid continental climate with no significant difference in precipitation between seasons (climate type Dfa, according to the Köppen–Geiger climate classification [24]). The site is devoted to the characterisation of the atmosphere using a synergy of active and passive remote sensing instruments along with modelling and satellite data ([25–28]). The state-of-the-art instruments located at MARS are further used in this study.

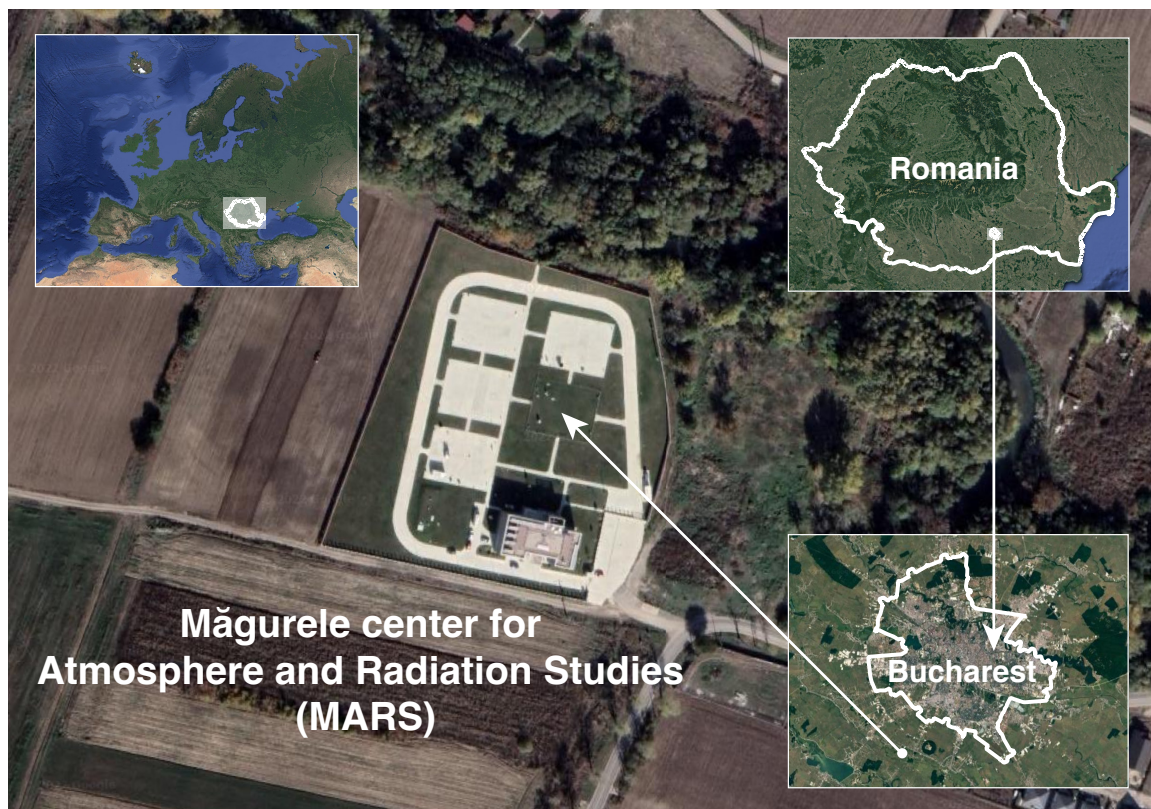


Figure 1. The location of the Măgurele centre for Atmosphere and Radiation studies (MARS) with respect to Bucharest. Based on Google Maps (map data: Google, Maxar Technologies) processed on QGIS [29].

2.1. Cloud Radar

The W-band cloud radar is a Frequency-Modulated Continuous Wave (FMCW) Doppler cloud radar [30], manufactured by Radiometer Physics GmbH (RPG), Germany, which was installed at MARS in November 2019 for continuous observations of the macrophysical and microphysical properties of clouds (Figure 2a). The cloud radar was deployed at MARS for the FRM4RADAR project (<https://geomt.uni-koeln.de/forschung/frm4radar>, accessed on 4 April 2022) with the aim of providing, as a part of a network, reference measurements for the EarthCARE satellite mission.

During the study period, the radar was operated with a 4-chirp sequence covering the height range 100–15000 m (Table 1). Between May 2020 and May 2021 vertical profiles were produced continuously (with occasional small gaps due to power outages and calibration) with a temporal resolution of 2.97 s and a spatial resolution varying from 27.1 m between 108 and 1100 m in altitude to 51.1 m between 10,016 and 14,973 m in altitude (Table 2). Before this period, the radar was operated with a 4-chirp sequence covering the height range 119–13,131 m (December 2019–May 2020) (Table 2). The radar was calibrated as recommended by manufacturer using an absolute calibration with liquid nitrogen every six months during the studied period.

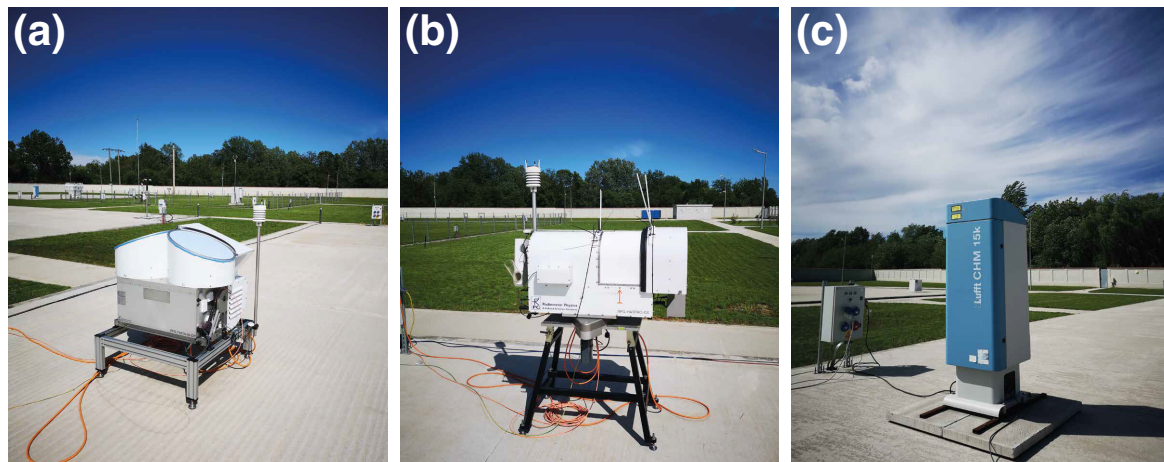


Figure 2. Instruments installed at the Măgurele Centre for Atmosphere and Radiation studies (MARS) used in this study: (a) 94 GHz RPG cloud radar, (b) HATPRO radiometer, and (c) CHM15k ceilometer.

Table 1. MARS instrument setup for the study period.

Instrument	Measured Parameters	Temporal Resolution	Spatial Resolution	Retrieved Parameters
RPG 94 GHz cloud radar	Doppler spectrum reflectivity LWP at 89 GHz	4.96 s 2.97 s (see Table 2)	29.8–42.1 m 27.1–51.1 m (see Table 2)	cloud presence and boundaries
HATPRO G5 microwave radiometer	brightness temperatures	60 s	column integrated measurements	liquid water path
CHM 15K ceilometer	profiles of attenuated backscatter coefficient	30 s	15 m	cloud base height

Figure 3 provides Contoured Frequency by Altitude Diagrams (CFADs, [31]) of reflectivity and Doppler velocity retrieved by the cloud radar during the entire observation period. The jumps in the distribution at specific altitudes are the direct result of the change in settings from chirp to chirp, with, for example, better vertical resolution being associated with lower sensitivities [30]. The maximum reflectivity density is situated in the -25 – -45 dBZ interval and within the 1 km closest to the ground. Separate to this peak in reflectivity density, there is also a distinct pattern of high reflectivity density for which the peak in reflectivity values decreases with altitude (from 10 dBZ near the ground to -25 dBZ at 9 km altitude). The Doppler velocity is mainly negative (i.e., falling towards the radar) above a 3 km altitude, ranging from -1 m s $^{-1}$ at 3 km in altitude to -0.1 m s $^{-1}$ at 10 km in altitude. Below 3 km in altitude, the Doppler velocity varies from -4 m s $^{-1}$ (due to large precipitating hydrometeors) to 2 m s $^{-1}$ (small hydrometeors experiencing thermal updrafts from convection in the planetary boundary layer [32]).

Table 2. MARS 94 GHz FMCW Doppler cloud radar chirp tables used between December 2019 and May 2021.

Attributes	1	2	3	4
Chirp sequence 1 used between December 2019 and May 2020				
Integration Time (s)	0.621	0.798	1.539	2.007
Range Interval (m)	100–1200	1200–4500	4500–6963	7000–13,152
Range Resolution (m)	29.8	29.8	29.8	42.1
Nyquist Velocity ($\pm m s^{-1}$)	10.5	8.2	5.8	4.5
Doppler FFT	1024	512	512	512
Total samples: 56,848,384	Total FFTs: 79,872		Total duration: 4.96 s	
Chirp sequence 2 used between May 2020 and May 2021				
Integration Time (s)	0.458	0.743	0.964	0.781
Range Interval (m)	100–1100	1100–5000	5000–10,000	10,000–15,000
Range Resolution (m)	27.1	30.4	31.1	51.1
Nyquist Velocity ($\pm m s^{-1}$)	8.4	6.6	5.1	4.2
Doppler FFT	1024	512	512	512
Total samples: 34,033,664	Total FFTs: 47,104		Total duration: 2.97 s	

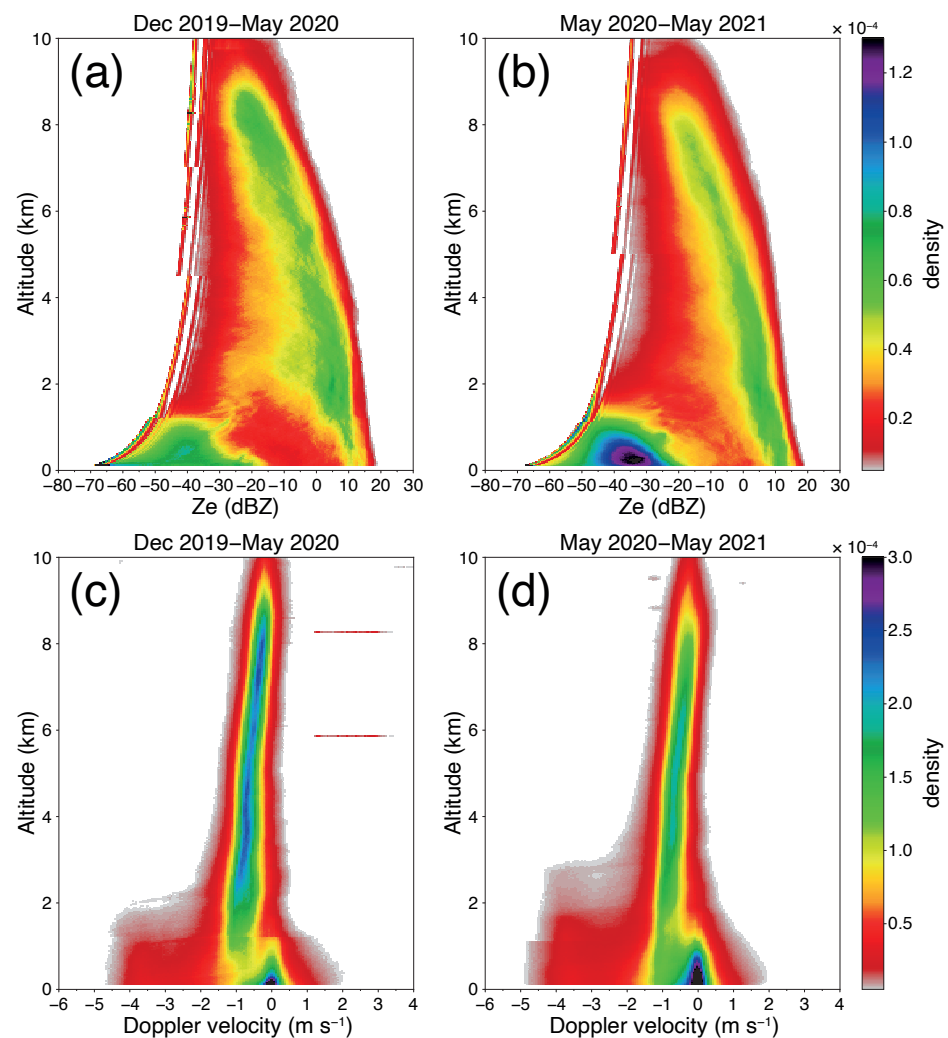


Figure 3. Contoured frequency by altitude diagrams (CFADs) of reflectivity (Z_e , dBZ) (a,b) and Doppler velocity (v , $m s^{-1}$) (c,d) for Dec 2019–May 2020 (a,c) and May 2020–May 2021 (b,d). These two periods correspond to the two chirp sequences described in Table 2 used during the study period. The probability density as a percentage is shaded according to the scale.

2.2. Microwave Radiometer

A 14-channel humidity and temperature microwave profiler (HATPRO G5 series, RPG, [33]), installed at MARS in November 2019, provided profiles of temperature, humidity, Integrated Water Vapor content (IWV) and Liquid Water Path (LWP) during the study period (Figure 2b). The temperature profiles were obtained with 10 min resolution and those of humidity with 1 min resolution. IWV and LWP are retrieved every minute [34]. HATPRO provides IWV observations with approximately $0.5\text{--}0.8\text{ kg m}^{-2}$ uncertainty [4] and LWP observations with a $20\text{--}30\text{ g m}^{-2}$ accuracy [34]. According to the manufacturer, temperature profiles have an accuracy of $\pm 0.6\text{ K RMS}$ ($0\text{--}2000\text{ m}$) and $\pm 1.0\text{ K RMS}$ ($>2000\text{ m}$) and the humidity profiles of $\pm 0.4\text{ g m}^3\text{ RMS}$. The retrieved profiles are provided with a vertical resolution varying from 30 m below 520 to 300 m between 6000 and 10,000 m; although, it should be noted that the true vertical resolution is lower than this [35,36]. The radiometer was calibrated as recommended by the manufacturer using an absolute calibration with liquid nitrogen every six months during the studied period, at the same time as the cloud radar.

2.3. Ceilometer Data

The CHM15k—Cloud Height Monitor up to 15 km altitude—ceilometer manufactured by Lufft (G. Lufft Mess-und Regeltechnik GmbH), installed at MARS in November 2019 [37], provided information about aerosols and clouds (droplets and ice crystals) (Figure 2c). The ceilometer is sensitive to high concentrations of cloud droplets and aerosols and thus can be used to detect liquid layers and cloud-base heights [38]. The instrument operates at a 1064 nm wavelength, with a 59.5 mW output power from a Nd:YAG solid-state, diode-pumped laser. The CHM15k ceilometer provides uncalibrated backscatter profiles up to 15,000 m with a vertical resolution of 15 m and a temporal resolution of 60 s.

2.4. Hydrometeors and Cloud Classification

The cloud classification used in this study was based on the target classification provided by the Cloudnet algorithm suite [9,11]. An example of the cloud radar data (i.e., radar reflectivity factor, Doppler velocity) and ceilometer data (i.e., attenuated backscatter coefficient) collected at the Bucharest–Măgurele Cloudnet station are shown in Figure 4a–c for 29 May 2020. Based on data retrieved by the cloud radar, microwave radiometer, and ceilometer, together with thermodynamic profiles from ECMWF, the Cloudnet algorithm suite returns the radar and lidar detection status and the target classification (Figure 4d,e). Furthermore, the radar data are corrected for liquid and gas attenuation in the Cloudnet algorithm suite. Thus, the ECMWF data are used together with LWP data to provide atmospheric profiles [11].

Vertical profiles containing the target classification above the Bucharest–Măgurele station were provided by Cloudnet every 30 s with a vertical resolution of 27–51 m (i.e., range bin) [39]. Between December 2019 (when the measurements started at the Bucharest–Măgurele station) and 31 May 2021 (when the cloud radar was deployed in Cape Verde for the international Aeolus Cal/Val Campaign, <https://askos.space.noa.gr/>, accessed on 17 March 2022), a total number of 1,327,680 profiles (84% of the total number of possible profiles during this period) were collected. Of the total number of profiles, 1,077,858 (81%) were profiles containing hydrometeors and 249,822 (19%) were clear-sky profiles. For the majority of months during the study period, the data availability was above 93%. The exceptions are for May (42% of the total number of possible profiles), June (30%), July (7%) 2020, and Sep 2020 (86%) (Figure 5).

Targets were classified as one of the following categories: (1) *cloud droplets*, (2) *drizzle or rain*, (3) *drizzle/rain and cloud droplets*, (4) *ice*, (5) *ice and supercooled droplets*, (6) *melting ice*, (7) *melting ice and cloud droplets*, (8) *aerosols*, (9) *insects*, or (10) *aerosols and insects* (Figure 6). These were then grouped into three categories (Figure 6): ice (category 4 from the Cloudnet target classification), liquid (categories 1, 2, and 3), and mixed-phase bins (categories 5, 6, and 7).

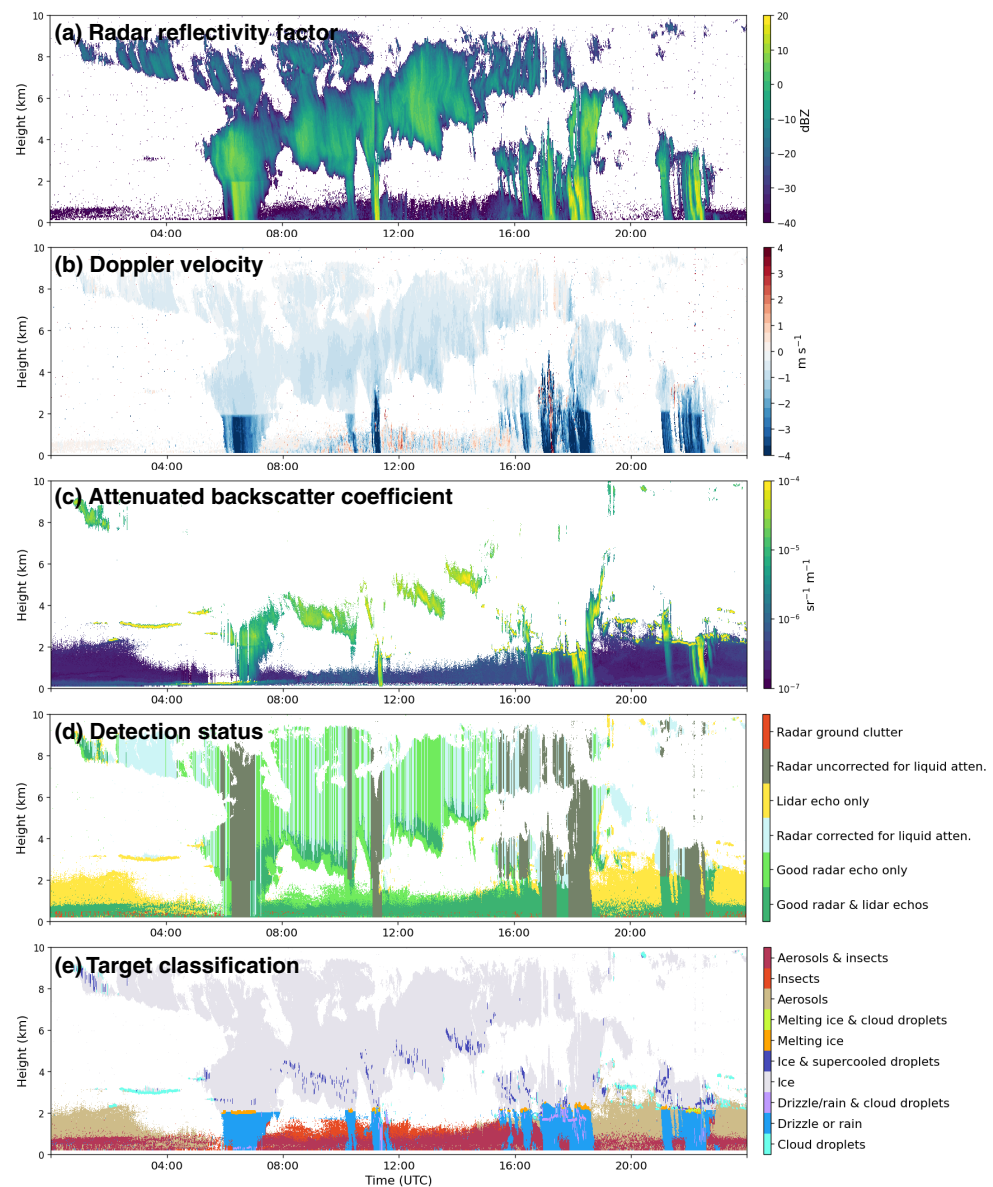


Figure 4. Time series of (a) radar reflectivity factor (dBZ), (b) Doppler velocity (m s^{-1}), (c) attenuated backscatter coefficient ($\text{sr}^{-1} \text{m}^{-1}$), (d) detection status, and (e) target classification based on the Cloudnet algorithm for 29 May 2020 between 0000 UTC and 2359 UTC. (Source <https://cloudnet.fmi.fi>, [39], accessed on 6 December 2021).

In this study, we define a cloud as having a layer of at least 5 consecutive height bins classified as meteorological targets (i.e., range bins classified as aerosols and/or insects were removed from the analysis) within an individual vertical profile. Thus, the minimum thickness of a classified cloud is 135–250 m (depending on the height bin resolution at a certain altitude (Table 2)). Each profile can have multiple cloud layers if the 5-bin height containing meteorological targets is separated by 5 bins classified as: *clear sky*, *aerosol particles*, *no cloud or precipitation*, *insects*, *no cloud or precipitation* or *aerosol coexisting with insects*, *no cloud or precipitation*. Cloud top and base height are then extracted for each cloud layer satisfying these conditions. Next, the cloud layers were classified based on the cloud type. Figure 6 shows the cloud categories adapted from [18], in which the clouds are classified as: ice only, mixed phase, precipitating mixed phase, liquid and precipitating liquid.

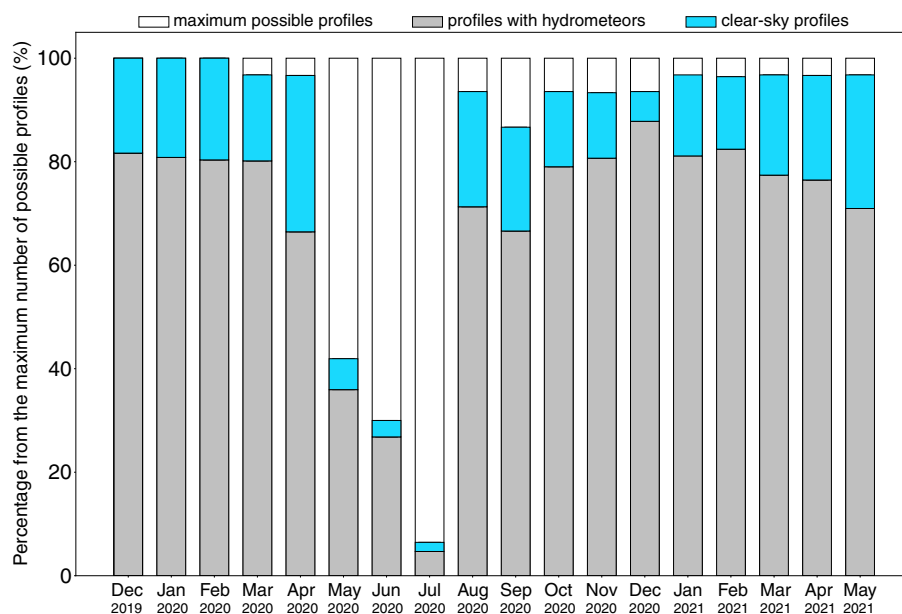


Figure 5. Data availability for the Bucharest–Măgurele station between December 2019 and May 2021. White bars represent the maximum possible number of vertical profiles for each month. The grey bars represent the number of profiles with hydrometeors, and the blue bars represent the number of clear-sky profiles (as a percentage of the total number of possible profiles).

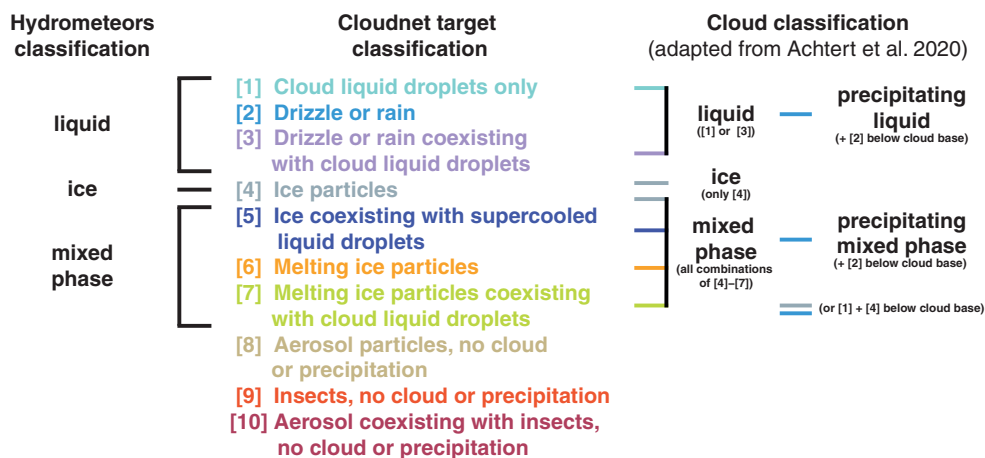


Figure 6. The Cloudnet target classification and the hydrometeors and cloud classification used in this study. The cloud classification is adapted from [18].

A cloud layer was classified as precipitating liquid cloud if the vertical range bins in the layer were *cloud liquid droplets only* or *drizzle or rain coexisting with cloud liquid droplets*, and the bins below the cloud base were classified as *drizzle or rain*. A mixed-phase precipitating cloud was defined in a similar manner; a mixed-phase cloud with *drizzle or rain* below the cloud base (Figure 6).

3. Results

We first summarise the thermodynamic conditions for the study period based on hourly profiles of cloud fraction, temperature, and relative humidity from the Integrated Forecasting System (IFS), the global operational numerical weather prediction model from the European Centre for Medium-Range Weather Forecasting (ECMWF) available from the Cloudnet database [40]. The data are available with a temporal resolution of one hour and a temporal resolution varying from 30 m at the ground level to 136 m at 15 km altitudes.

3.1. Environmental Characteristics

The mean monthly occurrence of cloud fraction from ECMWF-IFS shows high values over the entire column between Nov 2020 and Mar 2021 (Figure 7a). The annual cycle of temperature is characteristic of northern hemisphere mid-latitudes (Figure 7b). Close to the surface (<100 m in altitude), the lowest values for mean monthly temperature occurred in Jan 2020 (0.8 °C), and the highest value occurred in Aug 2020 (25.1 °C) (Figure 7b). At 5.5 km in altitude, the mean monthly temperature varied between −31.8 °C in Mar 2021 and −15.6 °C in Aug 2020. Relative humidity (with respect to water for temperatures above 0 °C, with respect to ice for temperatures below 0 °C) is shown in Figure 7c, and here, it should be noted that since the cloud physics scheme in a forecast model will generate clouds at relative humidities lower than the saturation value of 100%, a strong correlation between RH and clouds is not expected since the cloud physics scheme will also be taking into account other sub-gridscale processes (e.g., vertical motion). Close to the surface, the highest values of RH occurred during the winter months. In general, RH at low levels depends on the properties of the active surface layer [41]. High values of RH at upper levels (7–10 km) are associated with advection due to tropospheric circulations, such as moisture advection from the Mediterranean Sea [41].

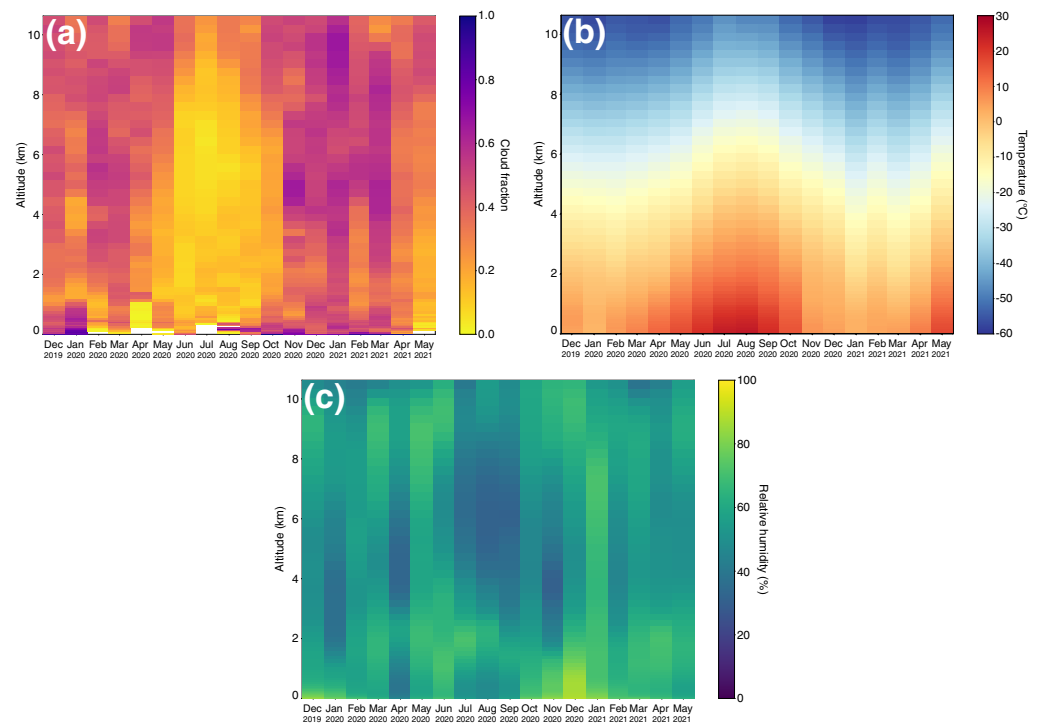


Figure 7. ECMWF-IFS monthly averages for (a) cloud fraction (>0.01), (b) temperature (°C), and (c) relative humidity (%) over MARS from December 2019 to May 2021.

3.2. Hydrometeor Characteristics

The monthly occurrence of hydrometeors as a function of altitude is shown in Figure 8. The majority of hydrometeors were observed below 5 km, with the exception of Jan and Mar 2021. Above 5 km, the frequency of occurrence is less than 20% (Figure 8a, left panel). The highest number of profiles with hydrometeors (>60%) were recorded in Dec 2020. As shown in Figure 8d (left panel), these were mainly liquid hydrometeors below 1 km. The lowest frequency (<20% over the entire column) was observed in Apr 2020, corresponding with low values for RH (Figure 7c). The analysis of clouds over Ny Ålesund, Svalbard [19], showed that the majority of hydrometeors were observed below 2 km with a maximum at 660 m.

The seasonal distribution of ice hydrometeors over the Bucharest-Măgurele Cloudnet station shows that this hydrometeor was most frequently (12–14%) observed between 2

and 4 km (Figure 8b). During winter seasons, the frequency of occurrence for ice hydrometeors was between 14 and 16%, with winter 2019–2020 having the maximum value around 2 km in altitude, and winter 2020–2021 having the maximum value around 3 km. The maximum between 2 and 4 km is mainly associated with clouds reaching in general 5–8 km and with the melting ice layer (as indicated by the Cloudnet algorithm) situated approximately at 2 km or with clouds producing snow (e.g., January 2021). This is also highlighted in Figure 9b, showing the distribution of the cloud base and cloud top for the winter and spring months. Spring 2020–2021 displayed a different distribution to the other seasons, with a maximum (16%) in the occurrence of ice hydrometeors at approximately 4.5 km and a secondary maximum (>14%) at approximately 9 km (mainly due to high frequencies of occurrence in May 2021). The maximum frequency of occurrence for mixed-phased hydrometeors was between 25 and 30% at 1–3 km, with the exception of Sep 2020–Feb 2021 (Figure 8c). For mixed-phase hydrometeors in autumn 2020, the maximum occurrence (17%) was observed at 2 km in altitude, while for winter 2021, the maximum occurrence (34%) was observed at around 1 km. The occurrence of hydrometeors during the Dec 2020–Feb 2021 winter period was dominated by Dec 2020 events. Liquid hydrometeors were mainly observed below 4 km in altitude, with maximum values of occurrence below 2 km (Figure 8d).

3.3. Cloud Characteristics

Figure 9 shows the distribution of cloud base height, cloud top height, and geometrical thickness for the five types of cloud layers analysed in this study (Figure 6).

For the studied region, the cloud spectrum varies from deep convective clouds reaching the tropopause during the warm season to shallow stratiform clouds during the cold season. Clouds were more frequently observed during winter (45% of all profiles) than in other seasons. Ice clouds were the most frequent type of cloud observed (468,463 profiles, 49.5% of all cloud profiles), followed by mixed-phase (220,280 profiles, 23.3%) and mixed-phase precipitable clouds (164,868 profiles, 17.4%). Liquid and liquid precipitable cloud profiles represented 5.1% and 4.5%, respectively, of the total number of cloud profiles. These results agree with those for the Eastern Mediterranean obtained by Marinou et al. [20], who showed that the most frequent type of clouds were ice clouds (41.8% of all cloud profiles) followed by mixed-phased clouds (12.2%). When compared with results from studies conducted in high latitudes [19], our results are not in agreement, as the most frequent type of clouds in high latitudes are mixed-phase clouds (20.6% of all single-layer clouds profiles), followed by ice (9%) and liquid clouds (6%).

The geometrical thickness of clouds over the Bucharest–Măgurele Cloudnet station varied from a median value of 244 m for liquid clouds during summer to 3362 m for mixed-phase precipitable clouds during spring. The minimum detected value for the geometrical thickness is between 135 and 155 m, given that a cloud layer is defined as at least five consecutive bins. For ice clouds, the distribution of these cloud properties does not change much between seasons, except for a slight increase in the cloud base height from winter (7994 m) to summer (9456 m). We should note that in the summer (4% of all available observations), the cloud classification was based on a smaller sample size compared with the other months. Mixed-phase precipitable clouds were deeper in spring and summer than in other months. Mixed-phase cloud thickness varied from 1218 m in winter to 792 m in autumn, with cloud base and cloud top heights increasing from winter to summer. The liquid cloud thickness varies by about 100 m from winter (358 m) to summer (244 m), and liquid precipitable clouds were deeper in summer than liquid clouds. For comparison, in the study of Arctic clouds by Achtert et al. [18], the thickness of liquid clouds varied little from summer to autumn. This is not in agreement with our results, which showed that the largest variation occurs from summer to autumn. Lower cloud top and cloud base heights were observed for mixed-phased and ice clouds in autumn than in summer for the Arctic, which is in agreement with our results. Concerning the cloud thickness, the results

obtained in this article agree well with those for the Eastern Mediterranean, where the cloud thickness was below 6 km for 74% of all clouds [20].

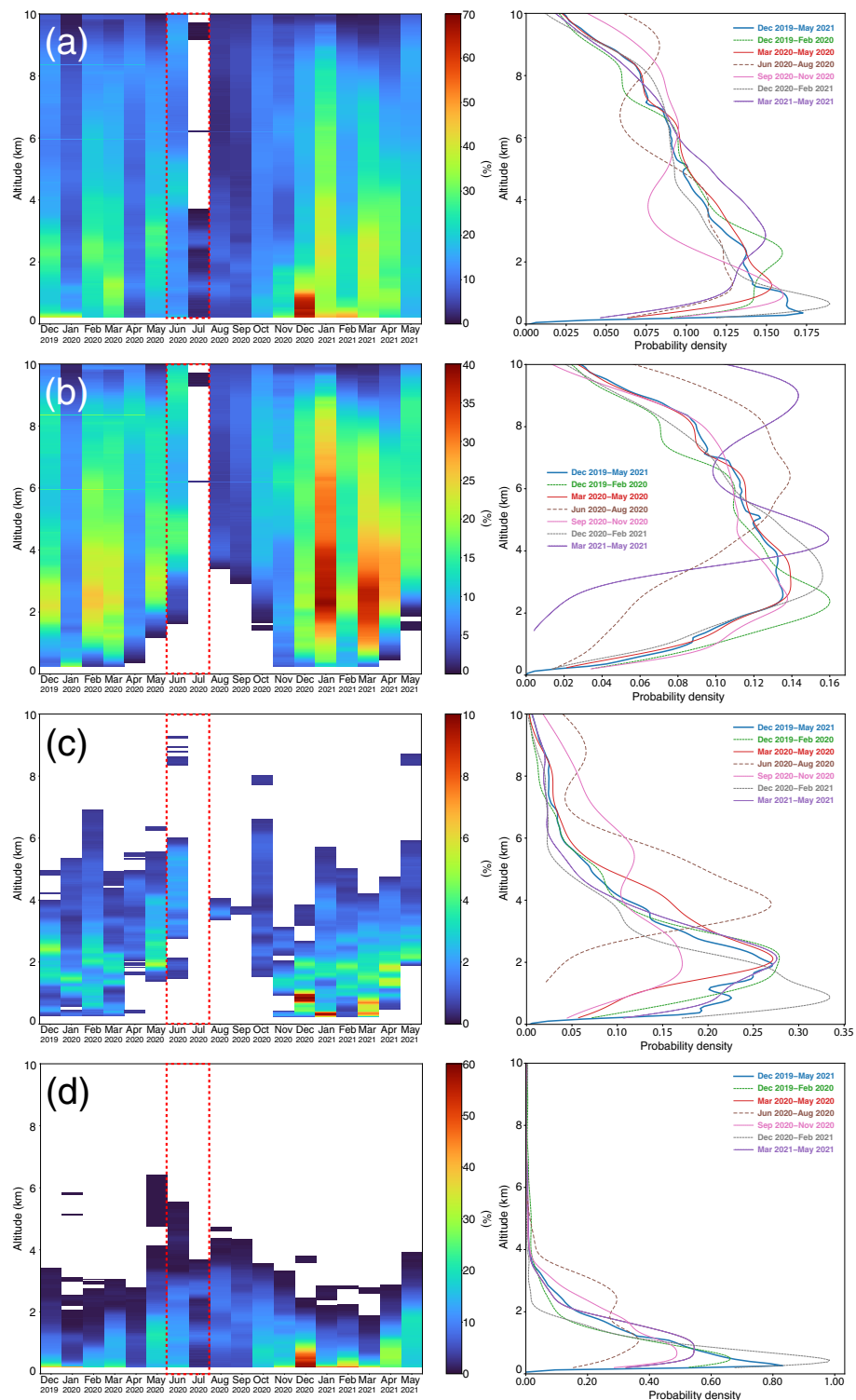


Figure 8. Frequency of occurrence for (a) liquid, mixed-phase and ice hydrometeors, (b) ice hydrometeors, (c) mixed-phase hydrometeors, and (d) liquid hydrometeors identified using the method proposed by [19] and based on target classification data from Cloudnet. The values are normalised to the total number of profiles for each month. The red dotted rectangle indicates the months with incomplete data (as shown in Figure 5). Left panels show the monthly distribution by altitude, and the right panels show the seasonal distribution by altitude.

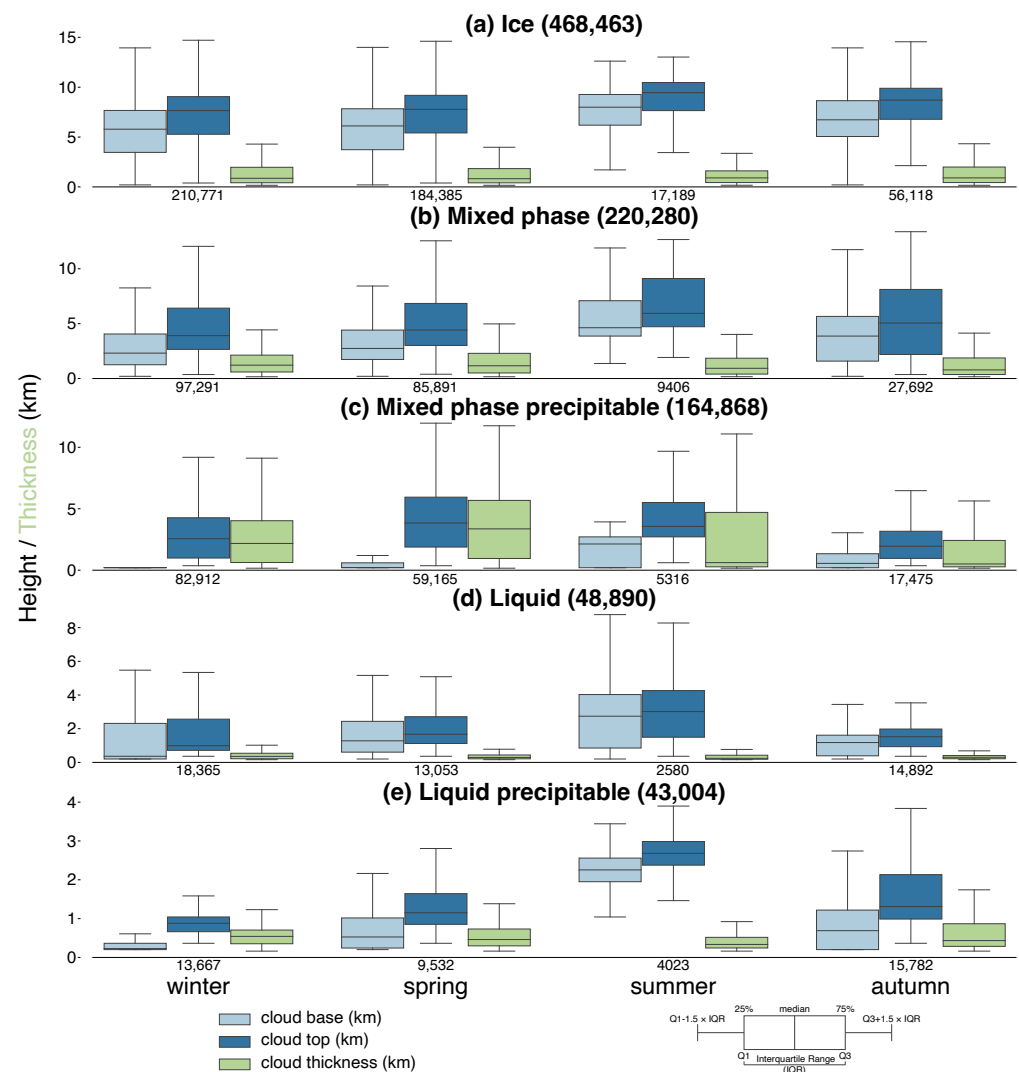


Figure 9. The seasonal occurrence of (a) ice, (b) mixed-phase, (c) mixed-phase precipitable, (d) liquid, and (e) liquid precipitable cloud as observed by the Bucharest–Măgurele Cloudnet station between Dec 2019 and May 2021. For each season, the distribution of cloud base height (in km, light blue), cloud top height (in km, blue), and cloud thickness (km, green) is presented as a box-and-whiskers plot. The number in each panel represents the total number of profiles for the type of cloud and for each season. Note that the data from summer and autumn are collected for one year, and for winter and spring, the data are collected for two years.

4. Conclusions

For the first time in Romania, cloud properties have been synergistically retrieved from the Bucharest–Măgurele Cloudnet station. The datasets were collected over a period of 18 months (Dec 2019–May 2021) in order to investigate the seasonal variations in cloud properties (i.e., phase, type). A total number of 1,327,680 profiles were analysed. The results indicate that clouds over the studied area were more frequently observed during winter (597,456 profiles) compared with other seasons. The most frequent type of clouds observed were ice clouds, followed by mixed-phase and mixed-phased precipitable clouds, totalling 853,611 profiles. Our results agree with those from previous studies, in particular for Eastern Mediterranean.

The results presented here are a baseline for future studies, which will focus on (1) better understanding the cloud properties over Bucharest–Măgurele using longer continuous datasets and including other properties (e.g., liquid water path); (2) the effect of the boundary layer structure on cloud evolution using measurements from a co-located Doppler wind

lidar; (3) the radiative properties of clouds using data from a co-located radiation station, which is part of the Baseline Surface Radiation Network; (4) the calibration and validation of products from future satellite missions, including the cloud profile measurements from EarthCARE.

Author Contributions: Conceptualisation, R.P. and D.E.; methodology, R.P. and B.A.; software, D.E. and M.B.; formal analysis, R.P., D.E. and B.A.; writing—original draft preparation, R.P., D.E., B.A. and E.O.; visualisation, D.E. and B.A.; supervision, S.Ş. and B.A.; funding acquisition, B.A. All authors have read and agreed to the published version of the manuscript.

Funding: This research was funded by the Romanian Ministry of Education and Research, CNCS-UEFISCDI (Project No. PN-III-P1-1.1-TE-2019-0649) within PNCDI III. Part of the work performed for this study was funded by (1) the Romanian National Core Program Contract No.18N/2019, and (2) the European Regional Development Fund through the Competitiveness Operational Programme 2014–2020, Action 1.1.3 Creating synergies with H2020 Programme, project Strengthen the participation of the ACTRIS-RO consortium in the pan-European research infrastructure ACTRIS, ACTRIS-ROC, MYSMIS code 107596 (contract No.337/2021). Further support was provided by the Romanian Ministry of Research, Innovation and Digitalisation, through Program 1—Development of the national research-development system, Subprogram 1.2—Institutional performance: Projects to finance the excellent RDI, Contract no. 18PFE/30.12.2021.

Data Availability Statement: The ground-based remote-sensing data used in this article are generated by the European Research Infrastructure for the observation of Aerosol, Clouds and Trace Gases (ACTRIS) and are available from the ACTRIS Data Centre using the following link: <https://hdl.handle.net/21.12132/2.909f7910cf684dc1>.

Acknowledgments: We acknowledge ACTRIS for providing the CLU (2022) dataset in this study, which was produced by the Finnish Meteorological Institute and is available for download from <https://cloudnet.fmi.fi/> (accessed on 1 December 2021). Measurements were supported by the European Space Agency through the FRM4RADAR project (ESA Contract No. 4000122916/17/I-EF). This article is also based on work from COST Action CA18235 PROBE, supported by COST (European Cooperation in Science and Technology) www.cost.eu (accessed on 31 March 2022). S.Ş. acknowledges the support from NO Grants 2014-2021, under Project EEA-RO-NO-2019-0423, contract no 31/01.09.2020. We also thank Simona Andrei, Mariana Adam, Florica Ţoancă, and Sorin Pîrloagă for their contribution to the maintenance of the instruments used in this article and Cristina Marin for her comments on the original draft.

Conflicts of Interest: The authors declare no conflict of interest.

References

1. Cesana, G.; Storelvmo, T. Improving climate projections by understanding how cloud phase affects radiation. *J. Geophys. Res.-Atmos.* **2017**, *122*, 4594–4599. [[CrossRef](#)]
2. Matus, A.V.; L'Ecuyer, T.S. The role of cloud phase in Earth's radiation budget. *J. Geophys. Res.-Atmos.* **2017**, *122*, 2559–2578. [[CrossRef](#)]
3. McFarquhar, G.M.; Bretherton, C.S.; Marchand, R.; Protat, A.; DeMott, P.J.; Alexander, S.P.; Roberts, G.C.; Twohy, C.H.; Toohey, D.; Siems, S.; et al. Observations of Clouds, Aerosols, Precipitation, and Surface Radiation over the Southern Ocean: An Overview of CAPRICORN, MARCUS, MICRE, and SOCRATES. *Bull. Am. Meteorol. Soc.* **2021**, *102*, E894–E928. [[CrossRef](#)]
4. Löhnert, U.; Schween, J.H.; Acquistapace, C.; Ebell, K.; Maahn, M.; Barrera-Verdejo, M.; Hirsikko, A.; Bohn, B.; Knaps, A.; O'Connor, E.; et al. JOYCE: Jülich Observatory for Cloud Evolution. *Bull. Am. Meteorol. Soc.* **2015**, *96*, 1157–1174. [[CrossRef](#)]
5. Haeffelin, M.; Barthès, L.; Bock, O.; Boitel, C.; Bony, S.; Bouniol, D.; Chepfer, H.; Chiriaco, M.; Cuesta, J.; Delanoë, J.; et al. SIRTa, a ground-based atmospheric observatory for cloud and aerosol research. *Ann. Geophys.* **2005**, *23*, 253–275. [[CrossRef](#)]
6. Stephens, G.; Winker, D.; Pelon, J.; Trepte, C.; Vane, D.; Yuhas, C.; L'Ecuyer, T.; Lebsock, M. CloudSat and CALIPSO within the A-Train: Ten Years of Actively Observing the Earth System. *Bull. Am. Meteorol. Soc.* **2018**, *99*, 569–581. [[CrossRef](#)]
7. Loeb, N.G.; Doelling, D.R.; Wang, H.; Su, W.; Nguyen, C.; Corbett, J.G.; Liang, L.; Mitrescu, C.; Rose, F.G.; Kato, S. Clouds and the Earth's Radiant Energy System (CERES) Energy Balanced and Filled (EBAF) Top-of-Atmosphere (TOA) Edition-4.0 Data Product. *J. Clim.* **2018**, *31*, 895–918. [[CrossRef](#)]
8. Mather, J.H.; Voyles, J.W. The ARM Climate Research Facility: A review of structure and capabilities. *Bull. Am. Meteorol. Soc.* **2013**, *94*, 377–392. [[CrossRef](#)]

9. Illingworth, A.J.; Hogan, R.J.; O'Connor, E.J.; Bouniol, D.; Brooks, M.E.; Delanoë, J.; Donovan, D.P.; Eastment, J.D.; Gaussiat, N.; Goddard, J.W.; et al. Cloudnet: Continuous evaluation of cloud profiles in seven operational models using ground-based observations. *Bull. Am. Meteorol. Soc.* **2007**, *88*, 883–898. [CrossRef]
10. Tukiainen, S.; O'Connor, E.; Korpinen, A. CloudnetPy: A Python package for processing cloud remote sensing data. *J. Open Source Softw.* **2020**, *5*, 2123. [CrossRef]
11. Hogan, R.J.; O'Connor, E.J. *Facilitating Cloud Radar and Lidar Algorithms: The Cloudnet Instrument Synergy/Target Categorization Product*; Cloudnet Documentation 14 pp; University of Reading: Reading, UK, 2004. Available online: <http://www.cloud-net.org/data/products/categorize.html> (accessed on 31 March 2022).
12. O'Connor, E.J.; Hogan, R.J.; Illingworth, A.J. Retrieving Stratocumulus Drizzle Parameters Using Doppler Radar and Lidar. *J. Appl. Meteorol.* **2005**, *44*, 14–27. [CrossRef]
13. Krasnov, O.A.; Russchenberg, H.W.J. A synergetic radar-lidar technique for the LWC retrieval in water clouds: Description and application to the Cloudnet data. In Proceedings of the 32d Conference on Radar Meteorology and 11th Conference on Mesoscale Processes, Albuquerque, NM, USA, 22–24 October 2005; p. 11R.7.
14. Hogan, R.J.; Mittermaier, M.P.; Illingworth, A.J. The retrieval of ice water content from radar reflectivity factor and temperature and its use in evaluating a mesoscale model. *J. Appl. Meteor. Climatol.* **2006**, *45*, 301–317. [CrossRef]
15. van Zadelhoff, G.J.; Donovan, D.P.; Klein Baltink, H.; Boers, R. Comparing ice cloud microphysical properties using CloudNET and Atmospheric Radiation Measurement Program data. *J. Geophys. Res.* **2004**, *109*, D24214. [CrossRef]
16. Bühl, J.; Seifert, P.; Myagkov, A.; Ansmann, A. Measuring ice- and liquid-water properties in mixed-phase cloud layers at the Leipzig Cloudnet station. *Atmos. Chem. Phys.* **2016**, *16*, 10609–10620. [CrossRef]
17. Wandinger, U.; Seifert, P.; Engelmann, R.; Bühl, J.; Wagner, J.; Schmidt, J.; Pospichal, B.; Baars, H.; Schwarz, A.; Kanitz, T.; et al. Observation of aerosol–cloud–turbulence interaction with integrated remote-sensing instrumentation. In Proceedings of the 9th International Symposium on Tropospheric Profiling, L'Aquila, Italy, 3–7 September 2012.
18. Achtert, P.; O'Connor, E.J.; Brooks, I.M.; Sotiropoulou, G.; Shupe, M.D.; Pospichal, B.; Brooks, B.J.; Tjernström, M. Properties of Arctic liquid and mixed-phase clouds from shipborne Cloudnet observations during ACSE 2014. *Atmos. Chem. Phys.* **2020**, *20*, 14983–15002. [CrossRef]
19. Nomokonova, T.; Ebell, K.; Löhnert, U.; Maturilli, M.; Ritter, C.; O'Connor, E. Statistics on clouds and their relation to thermodynamic conditions at Ny-Ålesund using ground-based sensor synergy. *Atmos. Chem. Phys.* **2019**, *19*, 4105–4126. [CrossRef]
20. Marinou, E.; Voudouri, K.; Tsikoudi, I.; Drakaki, E.; Tsekiri, A.; Rosoldi, M.; Ene, D.; Baars, H.; O'Connor, E.; Amiridis, V.; et al. Geometrical and microphysical properties of clouds formed in the presence of dust above the Eastern Mediterranean. *Remote Sens.* **2021**, *13*, 5001. [CrossRef]
21. Ștefan, S.; Ungureanu, I.; Grigoraș, C. A survey of cloud cover over Măgurele, Romania using ceilometer and satellite data. *Rom. Rep. Phys.* **2014**, *66*, 812–822.
22. Saftoiu Golea, G.L.; Ștefan, S.; Antonescu, B.; Iorga, G.; Livio, B. Characteristics of Stratocumulus clouds over Bucharest—Magurele. *Rom. Rep. Phys.* **2022**, *74*, 705.
23. Paraschivescu, M.; Râmbu, N.; Ștefan, S. Atmospheric circulations associated to the interannual variability of cumulonimbus cloud frequency in the southern part of Romania. *Int. J. Climatol.* **2012**, *32*, 920–928. [CrossRef]
24. Beck, H.; Zimmermann, N.; McVicar, T.; Vergopolan, N.; Berg, A.; Wood, E. Present and future Köppen–Geiger climate classification maps at 1-km resolution. *Sci. Data* **2018**, *5*, 1802214. [CrossRef] [PubMed]
25. Fragkos, K.; Antonescu, B.; Giles, D.M.; Ene, D.; Boldeanu, M.; Efstathiou, G.A.; Belegante, L.; Nicolae, D. Assessment of the total precipitable water from a sun photometer, microwave radiometer and radiosondes at a continental site in southeastern Europe. *Atmos. Meas. Tech.* **2019**, *12*, 1979–1997. [CrossRef]
26. Adam, M.; Stachlewska, I.S.; Mona, L.; Papagiannopoulos, N.; Bravo-Aranda, J.A.; Sicard, M.; Nicolae, D.N.; Belegante, L.; Janicka, L.; Szczepanik, D.; et al. Biomass burning events measured by lidars in EARLINET—Part 2: Optical properties investigation. *Atmos. Chem. Phys. Discuss.* **2021**, *2021*, 1–36. [CrossRef]
27. Nicolae, D.; Vasilescu, J.; Talianu, C.; Binietoglou, I.; Nicolae, V.; Andrei, S.; Antonescu, B. A neural network aerosol-typing algorithm based on lidar data. *Atmos. Chem. Phys.* **2018**, *18*, 14511–14537. [CrossRef]
28. Mărmureanu, L.; Marin, C.A.; Andrei, S.; Antonescu, B.; Ene, D.; Boldeanu, M.; Vasilescu, J.; Vițelaru, C.; Cadar, O.; Levei, E. Orange Snow—A Saharan Dust Intrusion over Romania During Winter Conditions. *Remote Sens.* **2019**, *11*, 2466. [CrossRef]
29. QGIS.org. QGIS Geographic Information System. QGIS Association. 2022. Available online: <http://www.qgis.org> (accessed on 5 July 2022).
30. Küchler, N.; Kneifel, S.; Löhnert, U.; Kollias, P.; Czekala, H.; Rose, T. A W-Band Radar–Radiometer System for Accurate and Continuous Monitoring of Clouds and Precipitation. *J. Atmos. Ocean. Technol.* **2017**, *34*, 2375–2392. [CrossRef]
31. Houze, R.A., Jr.; Wilton, D.C.; Smull, B.F. Monsoon convection in the Himalayan region as seen by the TRMM Precipitation Radar. *Quart. J. Roy. Meteor. Soc.* **2007**, *133*, 1389–1411. [CrossRef]
32. Ansmann, A.; Fruntke, J.; Engelmann, R. Updraft and downdraft characterization with Doppler lidar: Cloud-free versus cumuli-topped mixed layer. *Atmos. Chem. Phys.* **2010**, *10*, 7845–7858. [CrossRef]
33. Rose, T.; Crewell, S.; Löhnert, U.; Simmer, C. A network suitable microwave radiometer for operational monitoring of the cloudy atmosphere. *Atmos. Res.* **2005**, *75*, 183–200. [CrossRef]

34. Löhnert, U.; Crewell, S. Accuracy of cloud liquid water path from ground-based microwave radiometry: Part I. Dependency on cloud model statistics and precipitation. *Radio Sci.* **2003**, *38*, 8041. [[CrossRef](#)]
35. Cimini, D.; Hewison, T.J.; Martin, L.; Güldner, J.; Gaffard, C.; Marzano, F.S. Temperature and humidity profile retrievals from ground-based microwave radiometers during TUC. *Meteor. Z.* **2006**, *15*, 45–56. [[CrossRef](#)]
36. Löhnert, U.; Turner, D.D.; Crewell, S. Ground-based temperature and humidity profiling using spectral infrared and microwave Observations. Part I: Simulated retrieval performance in clear-sky conditions. *J. Appl. Meteor. Climatol.* **2009**, *48*, 1017–1032. [[CrossRef](#)]
37. Adam, M.; Fragkos, K.; Biniatoglou, I.; Wang, D.; Stachlewska, I.S.; Belegante, L.; Nicolae, V. Towards Early Detection of Tropospheric Aerosol Layers Using Monitoring with Ceilometer, Photometer, and Air Mass Trajectories. *Remote Sens.* **2022**, *14*, 1217. [[CrossRef](#)]
38. O'Connor, E.J.; Illingworth, A.J.; Hogan, R.J. A technique for autocalibration of cloud lidar. *J. Atmos. Ocean. Technol.* **2004**, *21*, 777–786. [[CrossRef](#)]
39. CLU. Cloud Profiling Product: Classification; 2019-12-01 to 2021-05-31; from Bucharest Romania. Generated by the Cloud Profiling Unit of the ACTRIS Data Centre. 2022. Available online: <https://hdl.handle.net/21.12132/2.a83ab8e12c794345> (accessed on 1 December 2021).
40. CLU. ECMWF Model Data; 2019-12-01 to 2020-05-31; from Bucharest, Romania. Generated by the Cloud Profiling Unit of the ACTRIS Data Centre. 2022. Available online: <https://hdl.handle.net/21.12132/2.7bb01f12416849ea> (accessed on 1 December 2021).
41. Wypych, A.; Bochenek, B.; Różycki, M. Atmospheric Moisture Content over Europe and the Northern Atlantic. *Atmosphere* **2018**, *9*, 18. [[CrossRef](#)]